# Probing Charge Transport in $\pi$-Stacked Fluorene-Based Systems

**Veaceslav Coropceanu,*,† Tamaki Nakano,*,‡,§ Nadine E. Gruhn,^ Ohyun Kwon,†,# Tohru Yade,‡ Ken-ichi Katsukawa,‡ and Jean-Luc Brédas*,†**

*School of Chemistry and Biochemistry, Georgia Institute of Technology, Atlanta, Georgia 30332-0400, Graduate School of Materials Science, Nara Institute of Science and Technology (NAIST), Takayama-cho 8916-5, Ikoma, Nara 630-0101, Japan, and Department of Chemistry, The University of Arizona, Tucson, Arizona 85721-0041*

*Received: February 9, 2006; In Final Form: March 16, 2006*

The molecular parameters governing charge transport along a $\pi$-stacked fluorene chain in poly(dibenzofulvene) are studied by a joint experimental and theoretical approach involving high-resolution gas-phase photoelectron spectroscopy and quantum-mechanical methods. We specifically investigate the electronic couplings between fluorene moieties as well as the intramolecular reorganization energies, for both holes and electrons. Our results indicate that a $\pi$-stacked fluorene chain favors hole transport over electron transport. The values for electronic couplings and reorganization energies estimated here are compared with those derived recently for pentacene.

## Introduction

Much interest is currently devoted to the exploitation of functional organic molecular compounds and polymers as active elements in new generations of plastic (opto)electronic devices such as field-effect transistors (FET),[1−3] light-emitting diodes (LED),[4,5] or photovoltaic and solar cells.[6−8] A better understanding of the charge-transport mechanism in these materials is key for the design of high-performance devices.

The highest carrier mobilities reported to date have been obtained in single crystals of oligomers with a herringbone-type solid-state packing. Pentacene, the major representative of such materials, displays a high hole mobility (reported to be as high as 35 $cm^2/Vs$ at room temperature),[9] even though the edge-to-face orientation typical of the herringbone packing does not provide for optimal intermolecular $\pi$-orbital overlap, which is a critical factor impacting the intrinsic carrier mobility. Many attempts have been made to improve the charge-transport properties of pentacene-like materials via substitution or functionalization.[10,11] Another strategy that currently receives increasing consideration is to exploit the interactions between extended $\pi$-electron systems as a driving force to generate supramolecular structures with a noncovalent $\pi-\pi$ stacking motif.[12−22] It is also important to note that noncovalent interactions between aromatic rings are key elements of numerous chemical and biological recognition processes;[23] they also influence the structure of proteins and DNA and control charge transport in DNA across the $\pi$-stacked bases.[24−26]

Recently, some of us reported the synthesis and characterized the properties of poly(dibenzofulvenes), poly(DBFs). These compounds present a stable $\pi$-stacked structure with all-trans main-chain C−C bonds and stacked side-chain fluorene chromophores; see Figure 1.[15−18]

Kim et al. [22] have investigated the structural and optical properties of several DBF oligomers by means of ab initio calculations. These authors also discussed the charge-transport properties of these systems; based on the shape of the frontier orbitals, they concluded that, in a poly(DBF)-like chain, transport is much more favorable for electrons than for holes. However, a detailed investigation of the molecular parameters that control the efficiency of charge transport in these systems is still missing. Here, we report on the electronic and vibrational couplings related to both electron and hole transport along a poly(DBF) chain.

## Model

In the simplest approximation, a poly(DBF) chain can be considered as an infinite one-dimensional stack of fluorene moieties. In perfectly ordered materials, charge transport can be described in terms of a band-like regime. In this case, the charge carrier, characterized with effective mass, $m_{eff}$, moves as a delocalized plane wave. This coherent motion is, however, perturbed by interactions with intra- and intermolecular vibrations. Generally speaking, the effective mass of the carriers and the electron−vibration coupling should be small to ensure an efficient charge transport. Within a simple tight-binding model, the total conduction [valence] bandwidth ($W_b$) and the effective mass of the electron [hole] of a poly(DBF) chain are defined by the electronic coupling (transfer integral, $t$) between adjacent fluorene units as $W_b = 4t$ and $m_{eff} = \hbar^2/2at$, respectively (here $\hbar$ is the reduced Planck's constant and $a$ is the spacing between the fluorene units). When the electronic interactions are comparable or weaker than the electron−vibration interactions, which is a common situation in organic semiconductors, a band-like regime is expected to take place only in perfectly ordered systems at very low temperatures. With increasing temperature, the bandwidth is gradually reduced by electron−phonon interactions.[27,28] This leads to an increase in effective mass and

* To whom correspondence should be addressed. E-mail: veaceslav.coropceanu@chemistry.gatech.edu; jean-luc.bredas@chemistry.gatech.edu; nakanot@eng.hokudai.ac.jp.
† Georgia Institute of Technology.
‡ Nara Institute of Science and Technology.
§ Present address: Graduate School of Engineering, Hokkaido University, Sapporo 060-8628, Japan.
^ The University of Arizona.
# Present address: Samsung Advanced Institute of Technology, San 14-1, Nongseo-Dong, Giheung-Gu, Yongin-Si, Gyeonggi-Do, Korea.

10.1021/jp060855j CCC: $33.50 
Published on Web 04/27/2006

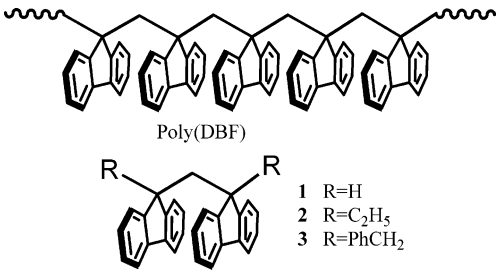


**Figure 1.** Chemical structure of the poly(DBF) chain and the dimers **1**−**3**.

consequently to charge localization. The motion of the carriers in this case can be modeled as a sequence of uncorrelated hops.[28] At the microscopic level, a hopping event can be described as a self-exchange electron-transfer (ET) reaction from a charged, relaxed unit to an adjacent neutral unit. The carrier mobility is then controlled by the self-exchange ET rate. At high temperature, when semiclassical ET theory usually applies, the self-exchange electron-transfer (hopping) rate is given by[27−30]

$$k_{ET} = A \exp\left[-\frac{\lambda}{4k_B T}\right] \quad (1)$$

Prefactor $A$ depends on the strength of the electronic coupling: in the case of weak coupling (nonadiabatic ET regime), $A \approx t^2$; in the case of relatively large coupling (adiabatic ET regime), $A = \nu_n$, where $\nu_n$ is the frequency for nuclear motion along the reaction coordinate.[29] The reorganization energy, $\lambda$, measures the strength of hole−vibration or electron−vibration interactions.[30−32] Thus, in both band-like and hopping regimes, there are two major parameters that impact the charge mobility: (i) the intermolecular transfer integral $t$, which should be maximized, and (ii) the reorganization energy $\lambda$ (electron−vibration coupling), which needs to be small for efficient transport.

The reorganization energy, $\lambda$, results from the molecular geometry modifications that occur when an electron is added to or removed from a chain unit (inner reorganization) as well as from the modifications in the surrounding medium due to polarization effects (outer reorganization). Here, we focus on the intramolecular contribution to $\lambda$. As discussed elsewhere in more detail,[30−32] the intramolecular reorganization energy consists of two terms corresponding to the geometric relaxation energies ($\lambda_{rel}^{(1)}$ and $\lambda_{rel}^{(2)}$) when going from the neutral-state geometry to the charged-state geometry and vice versa, see Figure 2. These two energy terms have been computed here directly from the adiabatic potential energy surfaces, as shown in Figure 2 (for more details, see refs 30−32).

In a tight-binding model, the total valence and conduction bandwidths ($W_b = 4t$) of an infinite one-dimensional stack result from the interaction of the HOMO (highest occupied molecular orbital) and LUMO (lowest unoccupied molecular orbital) levels of all individual units; the related energy splitting in a dimer corresponds to $2t$. In the case of symmetric dimers, this result is frequently used to obtain a simple (and often reliable) estimate of the transfer integral. Thus, the absolute value of the transfer integral for electron [hole] transfer can be obtained from the energy difference, $t = (\epsilon_{L+1[H]} - \epsilon_{L[H-1]})/2$, where $\epsilon_{L[H]}$ and $\epsilon_{L+1[H-1]}$ are the energies of LUMO and LUMO+1 [HOMO and HOMO−1] orbitals taken from the closed-shell configuration of the neutral state of a dimer.[33,34] In the same context, the energy splitting $\Delta E_{H/H-1} = \epsilon_H - \epsilon_{H-1}$ and, consequently, the electronic coupling related to hole transport can be estimated experimentally from the splitting between the first two ionization potentials (IP) as $\Delta E_{H/H-1} = \Delta IP = IP_2 - IP_1$ (and $t = \Delta IP/2$), as obtained from gas-phase ultraviolet photoelectron spectroscopy measurements.[35−39] As we discuss below, this approach based on the splitting of orbital energies is applicable only to symmetric systems and, in general, should be modified to account for asymmetry effects. Here, we investigate the couplings between fluorenes in the case of the three dimer systems, **1**−**3** (see Figure 1).

## Experimental and Computational Section

Compounds **1**−**3** have been synthesized according to published procedures.[15,17] Gas-phase photoelectron spectra of **1**−**3** were collected using an instrument and experimental procedures described in more detail elsewhere.[40] All samples have been sublimed below 200 °C with no evidence of contaminants present in the gas phase during data collection. The instrument resolution during data collection was better than 35 meV (measured using the full-width-at-half-maximum for the $^2P_{3/2}$ ionization of Ar). The valence ionization bands are represented analytically with the best fit of asymmetric Gaussian peaks. Each Gaussian peak is defined by four degrees of freedom: position, intensity, half-width to the high binding energy side, and half-width to the low binding energy side. The widths listed in Table 1 are the sum of the two individual half-widths. The peak positions and half-widths are reproducible to about ±0.02 eV.

The geometry of the fluorene monomer and dimers **1**, **2**, and **3** were optimized at both the density functional theory (DFT) B3LYP/6-31G** and semiempirical Austin model 1 (AM1) levels. The geometry of a DBF dimer was also optimized as a function of the dihedral angle between the two fluorene units, where the relative orientation of the two fluorenes was fixed and all the other geometrical parameters were relaxed. All DFT calculations were performed with the Gaussian-98 program.[41] The transfer integrals were estimated from electronic structures calculated at the semiempirical intermediate neglect of differential overlap (INDO) level.[42,43]

## Results and Discussion

The gas-phase photoelectron spectra of **1**−**3** are shown in Figure 3; the details of the first ionizations are shown in Figure 4. The ionization potentials as derived from deconvolutions with Gaussian functions are given in Table 1. From Figures 3 and 4 and Table 1, it is seen that replacing the terminal H atom in **1** with a larger terminal group causes a significant decrease of $IP_1$ by 0.23 eV and 0.26 eV on going to **2** and **3**, respectively. The ΔIP splittings of 0.29 eV and 0.27 eV in **2** and **3** are also significantly larger than that of 0.13 eV observed in **1**.

Furthermore, the shape of the low-energy part of the photoelectron spectrum in **1** is also very different when compared to the spectra of **2** and **3**. We attribute the difference in energetic and spectroscopic properties of **1** with respect to **2** and **3**, to differences in their geometries. Indeed, crystal structure analyses[17] indicate that the geometry of a DBF dimer critically depends on the chemical composition of the terminal groups, R. For R = H (**1**), the fluorene moieties adopt an edge-to-face (T-shaped) configuration (see Figure 5); on the other hand, in **2** and **3**, the fluorenes display a $\pi$-stacked conformation, although slightly twisted from a perfect face-to-face orientation. The INDO calculations performed on the basis of the experimental geometries reveal that the $IP_1$ of **2** and **3** are smaller by about 0.2−0.3 eV than in **1**. We also note that if one of the fluorene moieties were twisted so that **1** adopts a similar $\pi$-stacked conformation as **2** and **3**, its $IP_1$ would decrease by 0.3 eV. These results along with the difference in the shape of

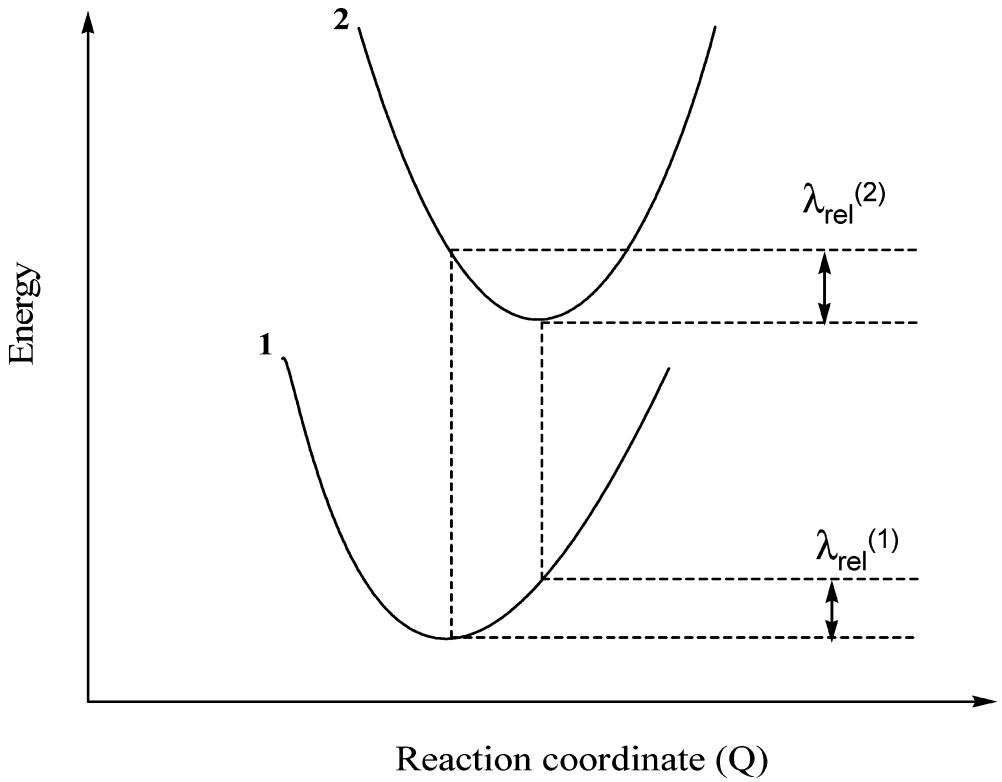


**Figure 2.** Sketch of the potential energy surfaces for the neutral state (**1**) and the charged state (**2**), showing the relaxation energies $\lambda_{rel}^{(1)}$ and $\lambda_{rel}^{(2)}$.

**TABLE 1: Fit Parameters of the Photoelectron Spectra for Fluorene Dimers 1, 2, and 3**

| position (eV) | half-width (eV) | | | relative peak area |
|---|---|---|---|---|
| | high | low | average | |
| | | **1** | | |
| 7.73 | 0.31 | 0.31 | 0.31 | 1 |
| 7.86 | 0.21 | 0.17 | 0.19 | 0.97 |
| 8.03 | 0.43 | 0.16 | 0.30 | 1.14 |
| 8.56 | 0.36 | 0.36 | 0.36 | 1.62 |
| 8.80 | 0.26 | 0.18 | 0.22 | 1.23 |
| 8.94 | 0.27 | 0.14 | 0.20 | 1.76 |
| 9.12 | 0.41 | 0.15 | 0.28 | 0.91 |
| 9.65 | 0.23 | 0.23 | 0.23 | 0.87 |
| 9.76 | 0.29 | 0.09 | 0.19 | 1.18 |
| 9.95 | 0.48 | 0.17 | 0.32 | 0.60 |
| | | **2** | | |
| 7.50 | 0.33 | 0.26 | 0.30 | 1 |
| 7.79 | 0.34 | 0.24 | 0.29 | 0.77 |
| 8.15 | 0.27 | 0.26 | 0.26 | 0.77 |
| 8.46 | 0.29 | 0.29 | 0.29 | 0.64 |
| 8.69 | 0.34 | 0.24 | 0.29 | 1.05 |
| 8.86 | 0.48 | 0.14 | 0.31 | 1.17 |
| 9.48 | 0.29 | 0.29 | 0.29 | 0.99 |
| 9.72 | 0.30 | 0.19 | 0.24 | 0.68 |
| | | **3** | | |
| 7.47 | 0.31 | 0.27 | 0.29 | 1 |
| 7.74 | 0.34 | 0.25 | 0.30 | 0.90 |
| 8.09 | 0.53 | 0.29 | 0.41 | 1.27 |
| 8.56 | 0.41 | 0.41 | 0.41 | 3.23 |
| 8.92 | 0.57 | 0.39 | 0.48 | 3.80 |
| 9.45 | 0.24 | 0.24 | 0.24 | 0.72 |
| 9.70 | 0.30 | 0.30 | 0.30 | 0.97 |

the photoelectron spectra suggest that systems **1**−**3** most likely possess similar geometries in the gas phase and in the crystalline state.

The INDO estimate of $\Delta E_{H/H-1} = 110$ meV in **1**, obtained on the basis of the experimental geometry, is in very good agreement with the measured value of 130 meV. However, the INDO estimates of 80 meV and 20 meV for $\Delta E_{H/H-1}$ in **2** and **3** are significantly smaller than the respective experimental values of 290 meV and 270 meV. At first glance, it would appear that the INDO estimates are in contradiction with the photoelectron data and with the general expectation that a $\pi-\pi$ stacked geometry, as in **2** and **3**, should lead to a larger $\Delta E_{H/H-1}$ splitting than the edge-to-face geometry of **1**. To better understand these results, we first note that, in general, the energy

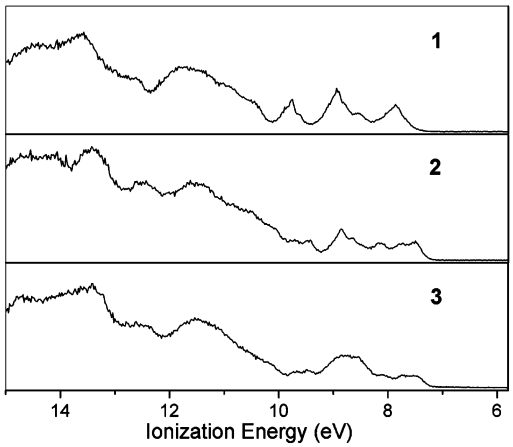


**Figure 3.** Gas-phase photoelectron spectra of compounds **1**−**3**.

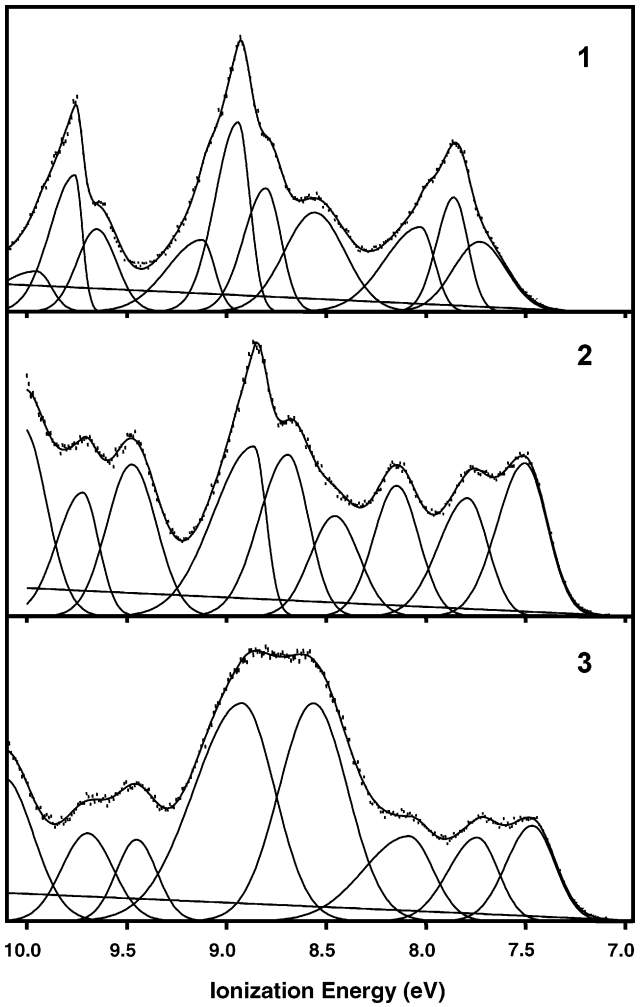


**Figure 4.** High-resolution close-up of the first ionizations of compounds **1**−**3**.

splitting $\Delta E_{H/H-1}$ depends not only on the transfer integral but also on the difference between energies $E_1$ and $E_2$ that correspond to two charge-localized configurations $M_a^+-M_b$ and $M_a-M_b^+$ of a dimer (where $M_a$ and $M_b$ are the constituent monomers). The parameters $\Delta E_{H/H-1}$, $\Delta E_0 = E_1 - E_2$ and $t$ are related via the following expression:[30]

$$\Delta E_{H/H-1} = \sqrt{(\Delta E_0)^2 + 4t^2} \qquad (2)$$

It is only in the case where the charged dimer is symmetric

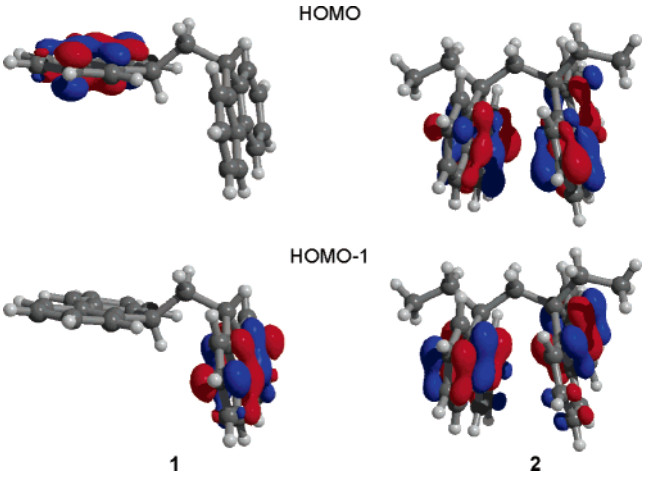


**Figure 5.** Pictorial representation of the INDO-calculated HOMO and HOMO−1 molecular orbitals (ions) in **1** and **2**. The molecular geometries depicted here come from crystal structures (ref 17).

(i.e., when the charge-localized configurations can be obtained from one another by a symmetry transformation) that $\Delta E_0 = 0$ and the resulting splitting is equal to $2t$. Even though in the present case all three systems are formed from chemically equivalent units, the edge-to-face orientation of the monomers in **1** results in the charge-localized states of $\mathbf{1}^{+\bullet}$ being asymmetric. The INDO calculations performed at experimental geometries (see also Figure 5) reveal that HOMO and HOMO−1 in **1** are entirely localized on a single fluorene unit. This means that the transfer integral in **1** is nearly zero and $\Delta E_{H/H-1}$ is only defined by $\Delta E_0$; thus, this system actually provides little insight about the electronic coupling in a poly(DBF) chain.

The situation is quite different in the case of systems **2** and **3**. As seen from Figure 5, HOMO and HOMO−1 in **2** are equally distributed over both monomers (HOMO and HOMO−1 in **3** show similar patterns). In this case, $\Delta E_0 = 0$ and $\Delta E_{H/H-1}$ is defined by the transfer integral. The apparent discrepancy between the INDO results and the photoelectron estimates of $\Delta E_{H/H-1}$ in **2** and **3** can be further explained by including the torsional motion into the model. Indeed, AM1 and DFT calculations[44] indicate that the neutral state of a $\pi$-stacked dimer is characterized by a rather flat potential surface with respect to the dihedral angle that measures the deviation from the cofacial orientation. As seen from Figure 6, and in agreement with the crystal structure data, the calculated adiabatic potential exhibits two minima that are separated by a very small barrier; the AM1 and DFT calculations yield values of 15 and 60 meV for the barrier, respectively. However, Figure 6 also shows that $\Delta E_{H/H-1}$ varies significantly with the dihedral angle: from zero around 30° (when the fluorene−fluorene orientation is close to that of the optimal geometry) to 0.5 eV when the dimer is in a perfect cofacial conformation. These findings, taken together, suggest that the experimental values of 290 and 270 meV for $\Delta$IP in **2** and **3** result from an averaging of $\Delta E_{H/H-1}$ over many dimer conformations with different dihedral angles. Consequently, we should expect that the maximum value of the electronic coupling is even larger than the 135−145 meV derived from the photoelectron measurements in **2** and **3**. In fact, by comparing the photoelectron spectrum of a phthalocyanine dimer with the absorption spectrum of its radical cation, Hush and co-workers[38] have recently shown that the electronic coupling derived from photoelectron measurements represents only about half the maximum value. Unfortunately, the radical-cation states of the present systems are not stable enough to allow a quantitative analysis of their optical spectra. We note,

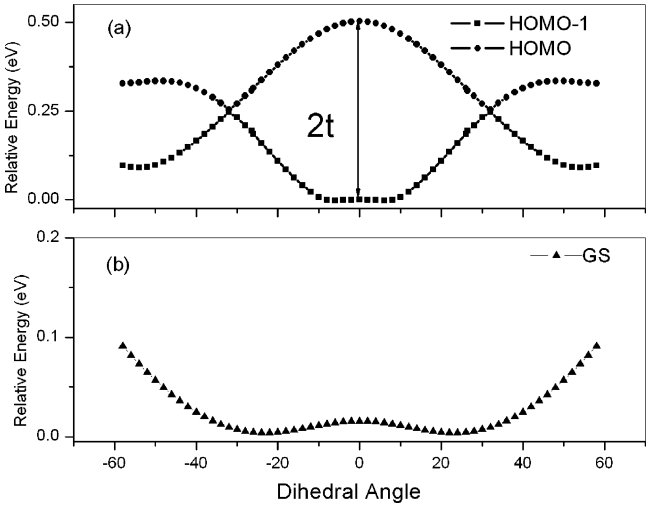


**Figure 6.** INDO-calculated energy splittings of the HOMO levels (a) and the ground-state adiabatic potential energy surface obtained at AM1 level (b) for a $\pi$-stacked dimer as a function of the dihedral angle (for a structural analogue of **2** and **3** with R = Me).

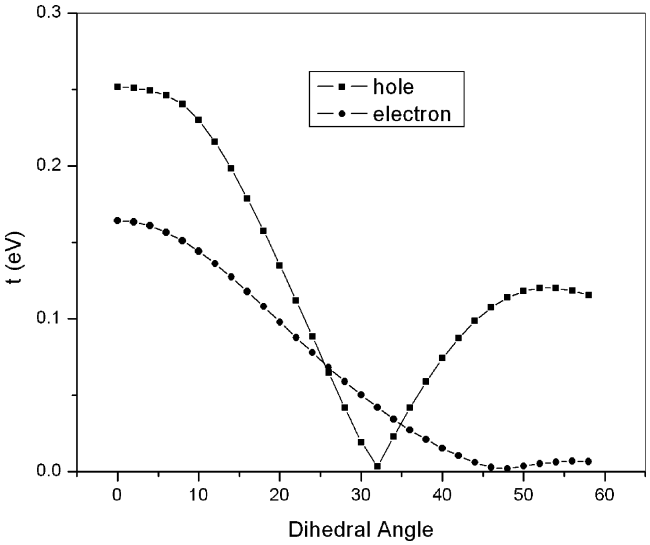


**Figure 7.** Evolution of the INDO-calculated transfer integrals (absolute values) for holes and electrons in a poly(DBF) chain as a function of the dihedral angle between adjacent fluorene units.

however, that the INDO estimate of 0.25 eV derived for a cofacial dimer is also nearly twice as large as the value derived from the photoelectron spectra. Thus, to summarize, our results suggest that the transfer integrals related to hole transport in a poly(DBF) chain can be as large as 0.2−0.3 eV. By comparison, we note that the respective transfer integrals estimated at the INDO level for pentacene crystals do not to exceed 0.1 eV.[45]

In Figure 7, we compare the electronic couplings in a poly(DBF) chain related to hole and electron transport. The electronic coupling for holes is generally larger than that for electrons; however, for a small range of dihedral angles around the potential minima this trend is reversed.

We also investigated the electron−vibrational and hole−vibrational couplings as coming from the reorganization energies, $\lambda$. Our DFT calculations yield values of 0.32 eV and 0.26 eV for the intramolecular reorganization energy related to electron and hole transport, respectively. We note that, in the context of small polaron theory, one-half of these values defines the corresponding polaron binding energies ($E_{pol} = \lambda/2$).[27,28,46] For comparison, $\lambda$ values in pentacene computed at the same level of theory are 0.132 eV and 0.097 eV.[30] Thus, our results indicate that holes in DBF chains are characterized by a larger transfer integral (bandwidth) and smaller reorganization energy (polaron binding energy) than electrons; charge transport along a poly(DBF) chain is therefore expected to be more efficient for holes than electrons.

## Conclusions

In this work, we used quantum-chemical calculations and gas-phase ultraviolet photoelectron spectroscopy measurements to characterize the two main parameters (i.e., reorganization energies and intermolecular transfer integrals) governing charge transport along a poly(DBF) chain. We have shown that electronic couplings between fluorene oligomers are larger for holes than for electrons. The intramolecular reorganization energy (or polaron binding energy) for holes is somewhat smaller than that for electrons. Consequently, in contrast to the recent conclusions by Kim et al.,[22] our results indicate that poly(DBF) chains favor hole transport over electron transport.

The estimated reorganization energies for both holes and electrons in poly(DBF) chains are about 2.5 times larger than in pentacene. The transfer integrals show a similar trend. This suggests that hole and electron mobilities along a poly(DBF) chain might tend toward those found in oligoacene systems.

**Acknowledgment.** The work at Georgia Tech is partly supported by the National Science Foundation, through the STC for Materials and Devices for Information Technology (DMR-0120967) and through Grant CHE-0343321, and by the Office of Naval Research. The work at Nara Institute of Science and Technology, Japan, is supported in part by Japan Science and Technology Agency (JST), the Ministry of Education, Culture, Sports, Science and Technology of Japan through Grant-in-Aid No. 16550110, Nippon Sheet Glass Foundation for Materials Science and Engineering, Iketani Science and Technology Foundation, and Sekisui Integrated Research (SIR).

## References and Notes

(1) Garnier, F.; Hajlaoui, R.; Yassar, A.; Srivastava, P. *Science* **1994**, *265*, 1684.
(2) Sirringhaus, H.; Tessler, N.; Friend, R. H. *Science* **1998**, *280*, 1741.
(3) Katz, H. E.; Lovinger, A. J.; Johnson, J.; Kloc, C.; Slegrist, T.; Li, W.; Lin, Y. Y.; Dodabalapur, A. *Nature* **2000**, *404*, 478.
(4) Burroughes, J. H.; Bradley, D. D. C.; Brown, A. R.; Marks, R. N.; Mackay, K.; Friend, R. H.; Burns, P. L.; Holmes, A. B. *Nature* **1990**, *347*, 539.
(5) Sheats, J. R.; Antoniadis, H.; Hueschen, M.; Leonard, W.; Miller, J.; Moon, R.; Roitman, D.; Stocking, A. *Science* **1996**, *273*, 884.
(6) Sariciftci, N. S.; Smilowitz, L.; Heeger, A. J.; Wudl, F. *Science* **1992**, *258*, 1474.
(7) Halls, J. J. M.; Walsh, C. A.; Greenham, N. C.; Marseglia, E. A.; Friend, R. H.; Moratti, S. C.; Holmes, A. B. *Nature* **1995**, *376*, 498.
(8) Yu, G.; Gao, J.; Hummelen, J. C.; Wudl, F.; Heeger, A. J. *Science* **1995**, *270*, 1789.
(9) Jurchescu, O. D.; Baas, J.; Palstra, T. T. M. *Appl. Phys. Lett.* **2004**, *84*, 3061.
(10) Anthony, J. E.; Brooks, J. S.; Eaton, D. L.; Parkin, S. R. *J. Am. Chem. Soc.* **2001**, *123*, 9482.
(11) Meng, H.; Bendikov, M.; Mitchell, G.; Helgeson, R.; Wudl, F.; Bao, Z.; Siegrist, T.; Kloc, C.; Chen, C. H. *Adv. Mater.* **2003**, *15*, 1090.
(12) Curtis, M. D.; Cao, J.; Kampf, J. W. *J. Am. Chem. Soc.* **2004**, *126*, 4318.
(13) Chesterfield, R. J.; Newman, C. R.; Pappenfus, T. M.; Ewbank, P. C.; Haukaas, M. H.; Mann, K. R.; Miller, L. L.; Frisbie, C. D. *Adv. Mater.* **2003**, *15*, 1278.
(14) Rathore, R.; Abdelwahed, S. H.; Guzei, I. A. *J. Am. Chem. Soc.* **2003**, *125*, 8712.
(15) Nakano, T.; Takewaki, K.; Yade, T.; Okamoto, Y. *J. Am. Chem. Soc.* **2001**, *123*, 9182.
(16) Nakano, T.; Yade, T.; Ishizawa, H.; Nakagawa, O.; Okamoto, Y. *Polym. Prepr. (Am. Chem. Soc., Div. Polym. Chem.)* **2002**, *43*, 609.
(17) Nakano, T.; Yade, T. *J. Am. Chem. Soc.* **2003**, *125*, 15474.

(18) Nakano, T.; Yade, T.; Yokoyama, M.; Nagayama, N. *Chem. Lett.* **2004**, *33*, 296.
(19) Scherlis, D. A.; Marzari, N. *J. Am. Chem. Soc.* **2005**, *127*, 3207.
(20) Lewis, F. D.; Kurth, T. L.; Delos Santos, G. B. *J. Phys. Chem. B* **2005**, *109*, 4893.
(21) Delos Santos, G. B.; Lewis, F. D. *J. Phys. Chem. A* **2005**, *109*, 8106.
(22) Kim, W. S.; Kim, J.; Park, J. K.; Mukamel, S.; Rhee, S. K.; Choi, Y. K.; Lee, J. Y. *J. Phys. Chem. B* **2005**, *109*, 2686.
(23) Meyer, E. A.; Castellano, R. K.; Diederich, F. *Angew. Chem.* **2003**, *42*, 1210.
(24) Schuster, G. B. *Acc. Chem. Res.* **2000**, *33*, 253.
(25) Lewis, F. D.; Letsinger, R. L.; Wasielewski, M. R. *Acc. Chem. Res.* **2001**, *34*, 159.
(26) O'Neill, M. A.; Barton, J. K. *J. Am. Chem. Soc.* **2004**, *126*, 11471.
(27) Pope, M.; Swenberg, C. E.; Pope, M. *Electronic processes in organic crystals and polymers*, 2nd ed.; Oxford University Press: New York, 1999.
(28) Silinsh, E. A.; Capek, V. *Organic molecular crystals: interaction, localization, and transport phenomena*; American Institute of Physics: New York, 1994.
(29) Demadis, K. D.; Hartshorn, C. M.; Meyer, T. J. *Chem. Rev.* **2001**, *101*, 2655.
(30) Brédas, J. L.; Beljonne, D.; Coropceanu, V.; Cornil, J. *Chem. Rev.* **2004**, *104*, 4971.
(31) Coropceanu, V.; Andre, J. M.; Malagoli, M.; Brédas, J. L. *Theor. Chem. Acc.* **2003**, *110*, 59.
(32) Malagoli, M.; Coropceanu, V.; da Silva Filho, D. A.; Brédas, J. L. *J. Chem. Phys.* **2004**, *120*, 7490.
(33) Newton, M. D. *Chem. Rev.* **1991**, *91*, 767.
(34) Kwon, O.; Coropceanu, V.; Gruhn, N. E.; Durivage, J. C.; Laquindanum, J. G.; Katz, H. E.; Cornil, J.; Brédas, J. L. *J. Chem. Phys.* **2004**, *120*, 8186.
(35) Paddon-Row: M. N. *Acc. Chem. Res.* **1982**, *15*, 245.
(36) Jordan, K. D.; Paddon-Row: M. N. *Chem. Rev.* **1992**, *92*, 395.
(37) Coropceanu, V.; Gruhn, N. E.; Barlow, S.; Lambert, C.; Durivage, J. C.; Bill, T. G.; Noll, G.; Marder, S. R.; Brédas, J. L. *J. Am. Chem. Soc.* **2004**, *126*, 2727.
(38) Binstead, R. A.; Reimers, J. R.; Hush, N. S. *Chem. Phys. Lett.* **2003**, *378*, 654.
(39) Hush, N. S. *Coord. Chem. Rev.* **1985**, *64*, 135.
(40) Cornil, J.; Gruhn, N. E.; dos Santos, D. A.; Malagoli, M.; Lee, P. A.; Barlow, S.; Thayumanavan, S.; Marder, S. R.; Armstrong, N. R.; Brédas, J. L. *J. Phys. Chem. A* **2001**, *105*, 5206.
(41) Frisch, M. J.; Trucks, G. W.; Schlegel, H. B.; Scuseria, G. E.; Robb, M. A.; Cheeseman, J. R.; Zakrzewski, V. G.; Montgomery, J. A., Jr.; Stratmann, R. E.; Burant, J. C.; Dapprich, S.; Millam, J. M.; Daniels, A. D.; Kudin, K. N.; Strain, M. C.; Farkas, O.; Tomasi, J.; Barone, V.; Cossi, M.; Cammi, R.; Mennucci, B.; Pomelli, C.; Adamo, C.; Clifford, S.; Ochterski, J.; Petersson, G. A.; Ayala, P. Y.; Cui, Q.; Morokuma, K.; Malick, D. K.; Rabuck, A. D.; Raghavachari, K.; Foresman, J. B.; Cioslowski, J.; Ortiz, J. V.; Stefanov, B. B.; Liu, G.; Liashenko, A.; Piskorz, P.; Komaromi, I.; Gomperts, R.; Martin, R. L.; Fox, D. J.; Keith, T.; Al-Laham, M. A.; Peng, C. Y.; Nanayakkara, A.; Gonzalez, C.; Challacombe, M.; Gill, P. M. W.; Johnson, B. G.; Chen, W.; Wong, M. W.; Andres, J. L.; Head-Gordon, M.; Replogle, E. S.; Pople, J. A. *Gaussian 98 (Revision A.11)*; Gaussian, Inc.: Pittsburgh, PA, 1998.
(42) Zerner, M. C.; Loew, G. H.; Kirchner, R. F.; Mueller-Westerhoff, U. T. *J. Am. Chem. Soc.* **1980**, *102*, 589.
(43) Ridley, J.; Zerner, M. *Theor. Chim. Acta* **1973**, *32*, 111.
(44) We note, however, that for a more reliable quantitative estimate of the activation barrier post Hartree−Fock calculations are, in general, needed.
(45) Cheng, Y. C.; Silbey, R. J.; da Silva Filho, D. A.; Calbert, J. P.; Cornil, J.; Brédas, J. L. *J. Chem. Phys.* **2003**, *118*, 3764.
(46) Holstein, T. *Ann. Phys. (N. Y.)* **1959**, *8*, 343.